NASA TECHNICAL NOTE

NASA TN D-2895

DETERMINATION OF MEAN ATMOSPHERIC DENSITIES FROM THE EXPLORER IX SATELLITE

by Gerald M. Keating, James A. Mullins, Claude W. Coffee, and David S. McDougal

Langley Research Center
Langley Station, Hampton, Va.

NATIONAL AERONAUTICS AND SPACE ADMINISTRATION • WASHINGTON, D. C. • JULY 1965

NASA TN D-2895

DETERMINATION OF MEAN ATMOSPHERIC DENSITIES FROM THE EXPLORER IX SATELLITE

By Gerald M. Keating, James A. Mullins, Claude W. Coffee, and David S. McDougal

Langley Research Center
Langley Station, Hampton, Va.

NATIONAL AERONAUTICS AND SPACE ADMINISTRATION

For sale by the Clearinghouse for Federal Scientific and Technical Information
Springfield, Virginia 22151 – Price $2.00

DETERMINATION OF MEAN ATMOSPHERIC DENSITIES FROM THE EXPLORER IX SATELLITE

By Gerald M. Keating, James A. Mullins, Claude W. Coffee,
and David S. McDougal
Langley Research Center

SUMMARY

A method is developed for determining mean atmospheric densities from changes in the orbital elements of the Explorer IX (1961 Delta 1) satellite, a 12-foot-diameter balloon. The decay of the total energy of the satellite orbiting about an oblate spheroid is evaluated and the energy change due to the work done by radiation force upon the satellite is subtracted to yield the energy decay attributed to atmospheric drag. The direct solar radiation force upon Explorer IX is determined from measured vectorial reflectances of the satellite material. Equations are given for the effective coefficient of drag of Explorer IX, and mean atmospheric densities at heights from 310 km to 765 km are tabulated for the entire lifetime of the satellite (February 1961 through March 1964) from changes in the orbital elements of Explorer IX.

Author

INTRODUCTION

Since the advent of earth satellites, there has been increased interest in, and opportunity for, measurement of atmospheric density at extreme altitudes. Besides the scientific value of using density data to obtain further physical insight into the nature of the atmosphere, the densities must be known in order to predict perturbations in the orbits of earth satellites and to predict satellite lifetimes. Because of the exceedingly low atmospheric densities at satellite altitudes, an indirect method is normally employed to infer the densities, namely: the density is deduced from the magnitude of atmospheric drag which is computed for the satellite from certain observed orbital perturbations. The Explorer IX (1961 Delta 1) satellite was designed with a low mass-area ratio exclusively for the measurement of atmospheric density by the indirect method.

Exactly how the general indirect method is applied depends upon the physical characteristics and orbital regime of the satellite. In this paper, the specific method used for determination of mean atmospheric densities from the Explorer IX satellite is developed and completely described and the densities thus obtained are tabulated so that interested parties may analyze them. Mean atmospheric densities in the vicinity of the satellite's perigee are

deduced from that portion of the energy decay of the satellite which is attributed to aerodynamic drag. Expressions and values are determined from the time rate of change of energy about an oblate spheroid in terms of mean elements, the total radiation force upon the satellite, the energy change due to radiation force, and the coefficient of drag averaged about one orbit.

In order to obtain mean atmospheric densities from the energy decay of other satellites the satellite mass, average cross section, perturbing forces effecting energy decay, thermal accommodation coefficient, satellite wall temperatures, and many other factors would have to be taken into account.

SYMBOLS

A area

$A_2 = J_2 r_E^2 = 66.0546$ km

a semimajor axis of osculating orbit averaged over 1 revolution

a_o semimajor axis of osculating orbit

$\overline{\Delta a_D}$ change in semimajor axis of orbit per revolution due to aerodynamic drag averaged over many revolutions

C_D aerodynamic drag coefficient

$\overline{C_D}$ effective aerodynamic drag coefficient

C_S solar constant at 1 astronomical unit

c speed of light in a vacuum

D aerodynamic drag

E energy

ΔE_D change in energy of satellite per revolution due to aerodynamic drag

$\overline{\Delta E_D}$ change in energy of satellite per revolution due to aerodynamic drag averaged over many revolutions

ΔE_S energy change of satellite per revolution due to solar radiation force

E_T total energy of satellite

ΔE_T total energy change of satellite

e eccentricity

$\vec{F}_S$ force exerted on satellite by direct solar radiation

$H = -\frac{\rho}{d\rho/dh}$

h height above earth

I incident power of light per unit area normal to direction of propagation

i orbit inclination referred to equatorial plane of date

J_2 coefficient of second harmonic in earth gravitational potential

K correction factor for rotation of atmosphere

$\vec{L}$ unit vector in direction of propagation of light

m satellite mass

n mean (anomalistic) motion

$P_{j,k}$ coefficients in expression for orbital elements

q_j generalized orbital elements

R perturbing potential

r distance from center of earth to satellite

r_E equatorial radius of earth

r_S distance from earth to sun in astronomical units

r_e distance from center of earth to point on shadow ellipse

r_{sat} radius of satellite

$\vec{r}(\beta)$ vectorial reflectance of surface for light incident at angle β

S molecular speed ratio

S_r molecular speed ratio of diffusely reflected particles

s arc of satellite orbit

$\dot{\vec{s}}$ satellite velocity

t	time
U	earth gravitational potential
V	potential energy of satellite
v	true anomaly
W	work
X,Y,Z	Cartesian coordinate axes
x,y,z	Cartesian coordinates
x_i	generalized rectangular coordinate
α	change in right ascension between ascending node and perigee point
α_S	right ascension of sun
α_p	right ascension of perigee
β	angle of incidence
δ_S	declination of sun
δ_p	declination of perigee
ϵ	eccentric anomaly
θ	angle measured in orbital plane from semimajor axis of shadow semi-ellipse about center of earth in direction of satellite motion to r_e
$\theta(\beta)$	angle between normal to area element and direction of vectorial reflectance
λ	angle measured at center of earth from ascending node of satellite orbit to earth-sun line
μ	product of universal gravitational constant and mass of earth
ν	angle between earth-sun line and its projection on orbital plane
ρ	atmospheric density
$\bar{\rho}$	mean atmospheric density
σ	standard deviation
τ	angle measured in direction of satellite motion from perigee to projection of earth-sun line on orbital plane

ϕ colatitude angle in spherical coordinate system

ψ azimuth angle in spherical coordinate system

Ω right ascension of ascending node referred to equinox of 1950.0

ω argument of perigee

Subscripts:

in shadow entry

out shadow exit

p at perigee

t at time t

EXPERIMENT DESCRIPTION

Because of the exponential decrease of atmospheric density with height, most of the change of energy due to atmospheric drag occurs in the vicinity of perigee for moderate orbital eccentricities. The higher the eccentricity of the satellite orbit, the greater is the portion of energy decay in the immediate vicinity of perigee, and, therefore, the more accurately the position of the density measurement may be pinpointed. The lower the mass-area ratio of the satellite, the greater is the variation of the orbit due to energy decay and, therefore, the more accurate the density may be measured.

In order to obtain accurate values for both the magnitude and position of a density determination, it was, therefore, advantageous to place a satellite with a low mass-area ratio into an eccentric orbit. The Explorer IX satellite (fig. 1) was designed specifically for this purpose. The 12.00-foot-diameter satellite weighed 14.62 pounds, had a lower mass-area ratio than all previous satellites except Echo I (1960 Iota), and yet was sturdy enough to remain spherical at heights above 150 km (ref. 1). Because it was spherical, the satellite presented the same known frontal area to the atmosphere regardless of its orientation. Also it could be tracked optically and by radar because of its shiny metallic surface. Furthermore, the lifetime of the experiment is not limited to electronic instrument lifetime but to satellite lifetime, because the entire satellite served as a sensor.

Explorer IX was launched on February 16, 1961, from the NASA Wallops Station by means of the solid-propellant Scout vehicle. The initial orbit had an inclination of 38.8°, a height of perigee of 632 km, and a height of apogee of 2586 km. It was predicted that such an orbit would be close to a resonant condition for radiation force which could substantially reduce the satellite lifetime. Therefore, the satellite was launched in the early morning, allowing the perigee altitude to increase for 1 year and to decrease for the next

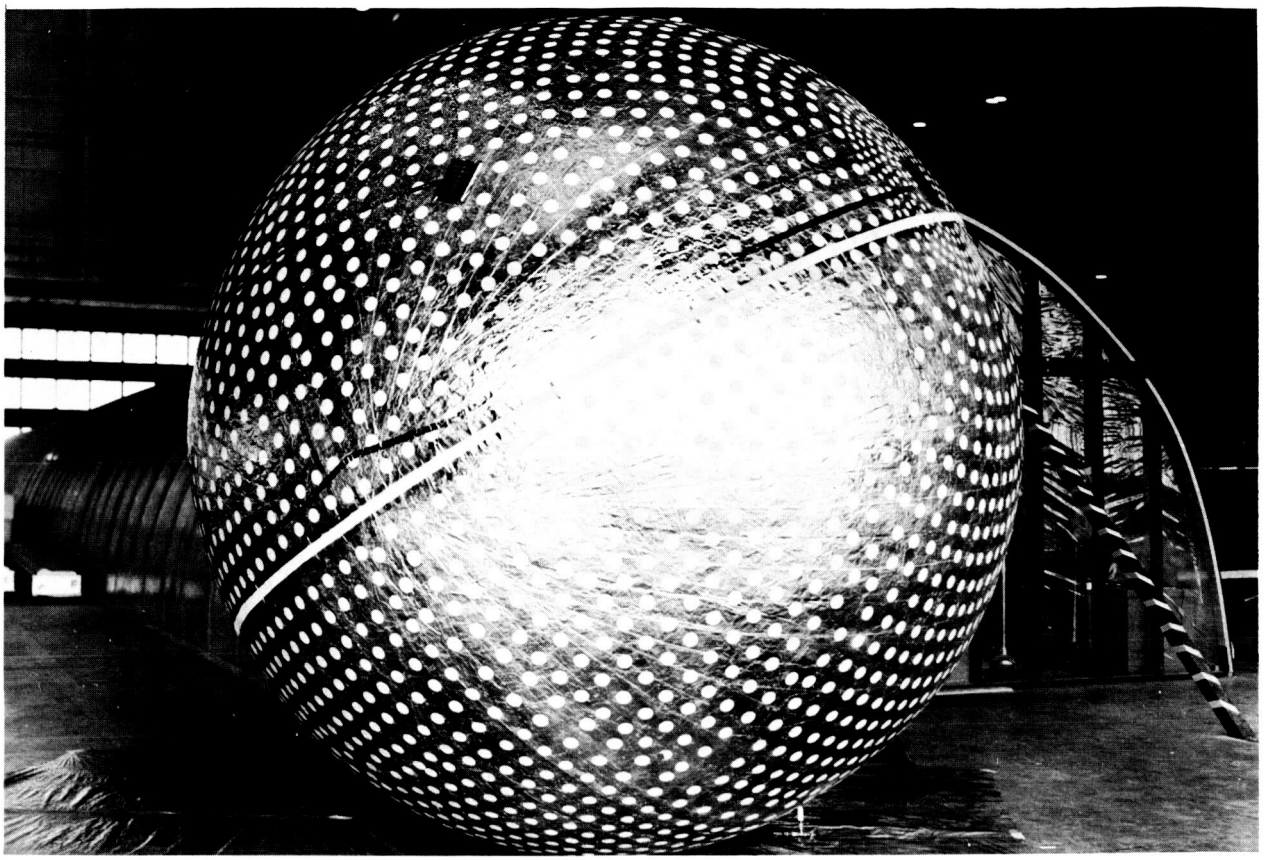

Figure 1.- Explorer IX satellite. L-61-3762

2 years. If an evening launch had been attempted, radiation force would have driven the satellite into the earth in less than a year. Besides increasing the satellite lifetime, a morning launch made it possible to obtain densities for the same altitude at two different times.

PROCEDURE

The procedure used to obtain mean atmospheric densities may be outlined as follows:

(1) Accurate observations of the satellite were continually obtained from various sources.

(2) Time-dependent orbital elements were calculated from these observations by means of a differential improvement program.

(3) The energy decay rate was deduced from the time-dependent orbital elements.

(4) By eliminating the computed energy changes due to forces other than atmospheric drag, the energy decay rate due to drag was deduced.

(5) A mean atmospheric density was deduced from the energy decay rate due to drag and certain aerodynamic properties of the satellite when certain properties of the atmosphere were assumed.

These steps are discussed in greater detail in the following sections.

Observations

The shiny metallic surface of the balloon permits both radar and optical tracking. The Baker-Nunn camera network and moonwatch teams were the primary sources of position measurements used to determine orbital elements. Publications are available which describe the Baker-Nunn cameras of the Smithsonian Institution Astrophysical Observatory (for example, ref. 2) and the methods of reduction of the photographs to position measurements (for example, ref. 3); therefore, only a brief discussion is given herein.

For bright satellites such as Explorer IX a fixed camera with a rotating barrel shutter is used. This shutter interrupts the trace of the satellite five times during an exposure (fig. 2). At the instant at which the central break occurs, the time is recorded on the film. Satellite direction relative to the star background at the time of the photograph is determined by measuring the center of the central break with respect to background star images. These observations are accurate to a few minutes of arc when field-reduced, and they are later reduced with accuracies of a few seconds of arc. (See ref. 3.) An average of about 1 observation per satellite revolution was obtained for the lifetime of the satellite. Another important source of observations is the numerous moonwatch teams throughout the world. Moonwatch observations, though accurate to only about 0.5°, are an important supplement to the Baker-Nunn data.

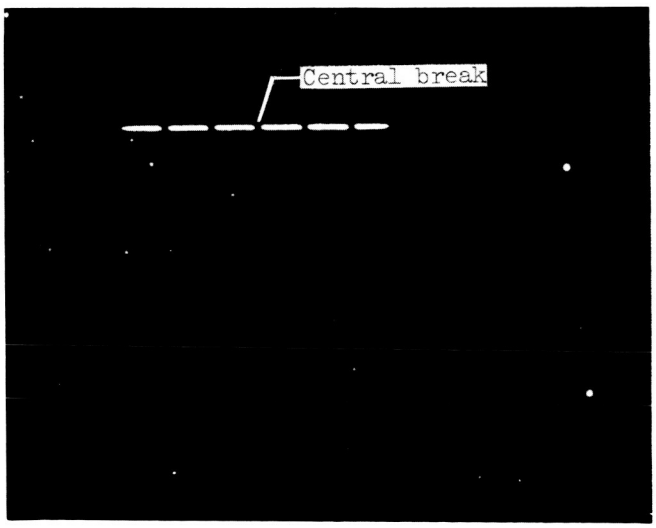

L-65-85

Figure 2.- Chopped trace of satellite image.

Determination of Orbits

The Smithsonian Astrophysical Observatory Differential Orbit Improvement Program (refs. 4 and 5) was used to determine the orbital elements of the satellite from the observations. The method of determination of the orbital elements is essentially as

follows. A set of expressions for the orbital elements is assumed. These elements vary with time and are composed of polynomials with the option of additional transcendental and exponential terms, such as

$$q_j = P_{j,1} + P_{j,2}t + P_{j,3}t^2 + P_{j,4}t^3 \tag{1}$$

where

q_j orbital elements

$P_{j,k}$ constants

t time from epoch

It is these constants $P_{j,k}$ which are to be improved.

The expressions for the elements are evaluated at times corresponding to the times at which observations were made and short-term gravitational perturbations (ref. 6) are added. The observations are transformed to rectangular sidereal coordinates and the computed satellite positions are compared with the observed positions. The residual from a given measurement can be equated with a linear combination of corrections for the elements. The partial derivatives of the rectangular coordinates with respect to the elements are coefficients in the following resultant relation:

$$(\Delta x_i)_t = \sum_j \left(\frac{\partial x_i}{\partial q_j}\right)_t \Delta q_j \tag{2}$$

where

x_i rectangular coordinate

$(\Delta x_i)_t$ residual in coordinate x_i at time t

The increments Δq_j can in turn be written as linear combinations of the error in the coefficients $P_{j,k}$ as follows:

$$\Delta q_j = \sum_k \left(\frac{\partial q_j}{\partial P_{j,k}}\right) \Delta P_{j,k} \tag{3}$$

If enough measurements are made, the corrections $\Delta P_{j,k}$ can be determined. In practice, many more observations are made than the minimum number necessary, and the corrections $\Delta P_{j,k}$ are determined by a method of least squares.

The standard deviation σ of the residuals is then computed and all measurements with residuals greater than 3σ are discarded. The entire process is

repeated until all the residuals are within the 3σ acceptable maximum. At this time the program prints out a set of parameters $P_{j,k}$.

In practice, least-mean-square fits devoid of short-periodic perturbations are found for eccentricity e, orbital inclination i, argument of perigee ω, right ascension of ascending node Ω, and mean anomaly M. The semimajor axis a is determined from the following relation (ref. 6):

$$a = \left(\frac{\mu}{n^2}\right)^{1/3}\left[1 - \frac{A_2}{3} a^{-2}\left(1 - e^2\right)^{-3/2}\left(1 - \frac{3}{2}\sin^2 i\right)\right]$$

where n, the mean (anomalistic) motion, is dM/dt. The elements derived by the above procedure are referred to as mean elements.

Satellite Energy in Terms of Mean Elements

A relationship between the energy of the satellite and the mean elements can be obtained in the following manner. The total energy of the satellite E_T is the sum of the kinetic energy $\frac{1}{2} m\dot{s}^2$ and the potential energy V. The kinetic energy for the osculating ellipse is given by $\frac{m\mu}{2}\left(\frac{2}{r} - \frac{1}{a_o}\right)$ and the potential energy due to the gravitational potential of the earth U is -Um, where

$$U = \frac{\mu}{r} + \mu\left\{\frac{A_2}{a_o^3}\left(\frac{a_o}{r}\right)^3\left[\frac{1}{3} - \frac{1}{2}\sin^2 i + \frac{1}{2}\sin^2 i \cos 2(\omega + v)\right]\right\} \tag{4}$$

and

$$R = U - \frac{\mu}{r} = \mu\left\{\frac{A_2}{a_o^3}\left(\frac{a_o}{r}\right)^3\left[\frac{1}{3} - \frac{1}{2}\sin^2 i + \frac{1}{2}\sin^2 i \cos 2(\omega + v)\right]\right\} \tag{5}$$

Then

$$E_T = \frac{1}{2}\mu m\left(\frac{2}{r} - \frac{1}{a_o}\right) - m\left(\frac{\mu}{r} + R\right) \tag{6}$$

or

$$E_T = -m\left(\frac{\mu}{2a_o} + R\right) \tag{7}$$

Equation (7) gives the energy for the osculating ellipse in terms of the osculating semimajor axis and the perturbing potential. If the satellite is

perturbed only by the oblateness potential, the energy for the osculating ellipse is constant and therefore equal to the energy for the mean ellipse. According to reference 6, the semimajor axis of the mean ellipse is related to the semimajor axis of the osculating ellipse by

$$a_o = a + \frac{A_2}{a_o}\left\{\frac{2}{3}\left(1 - \frac{3}{2}\sin^2 i\right)\left[\left(\frac{a_o}{r}\right)^3 - (1 - e^2)^{-3/2}\right] + \left(\frac{a_o}{r}\right)^3 \sin^2 i \cos 2(\omega + v)\right\} \tag{8}$$

Substitution of equation (8) and equation (5) into equation (7) yields

$$E_T = -\frac{\mu m}{2a}\left[1 + \frac{2A_2}{3a^2}\left(1 - \frac{3}{2}\sin^2 i\right)(1 - e^2)^{-3/2} + \ldots\right] \tag{9}$$

Energy changes in the orbit can be deduced from changes in the orbital elements. Since the energy change is observed to be small,

$$\Delta E_T = \frac{\mu m}{2a^2}\Delta a + \frac{\mu m A_2}{a^3}(1 - e^2)^{-3/2}\left[\sin i \cos i\, \Delta i - \left(1 - \frac{3}{2}\sin^2 i\right)(1 - e^2)^{-1} e \Delta e\right] \tag{10}$$

In the orbital regime of Explorer IX, the changes of e and i are small enough that the energy change may be approximated by the equation

$$\Delta E_T \approx \frac{\mu m}{2a^2}\Delta a \tag{11}$$

with errors of the order of J_2 or about 0.1 percent. Therefore, a change of energy may be measured in terms of a change in the mean semimajor axis.

Causes of Energy Change

In order to evaluate the energy change due solely to atmospheric drag, the energy changes due to other perturbing forces must be determined and subtracted from the total energy change.

Gravitational effects.- If the satellite is perturbed only by the earth gravitational field, the satellite total energy with respect to the earth remains constant. The lunar and solar gravitational perturbations may be assumed not to affect the semimajor axis (refs. 7 and 8). Therefore, from equation (11) the change in energy due to these effects is negligible.

Charge drag.- Because of the high thermal velocity of electrons relative to satellite velocity and the lower ion velocity, the satellite acquires a

negative charge which is decreased to some extent by photoemission. Consequently, ions which would not have been affected by a neutral satellite strike or are deflected by the satellite. The resulting drag, additional to that which would have been experienced by a neutral satellite, is referred to as electrostatic drag which has been estimated for the Explorer IX satellite (ref. 9) to be about 2 percent of the drag upon a neutral satellite at 1500 km for average solar activity with no photoemission assumed. Photoemission reduces the charge and therefore the relative effect of electrostatic drag. It should be noted that the percentage ionization decreases with decreasing solar activity and decreasing altitude. Since the perigee point of Explorer IX was continuously in the sunlight throughout its lifetime, and the solar activity and altitude were less than those assumed, it is believed that this effect would be less than 1 percent.

The satellite becomes polarized when cutting the earth's magnetic lines of force. With an increased electron flux on the positively charged side of the satellite and an increased ion flux on the negatively charged side, a current flows across the satellite which interacts with the earth's magnetic field to produce an induction drag. At 1500 km (ref. 9), the induction drag has been determined to be about 1 percent of the neutral drag. For the range of heights of the Explorer IX perigee, this effect is quite negligible. Therefore, the change of energy due to electrostatic and electromagnetic drag forces will lead to errors of less than 1 percent in atmospheric density.

Radiation forces.- Finally, the effects of radiation forces should be considered. The change of energy produced by direct solar radiation has been found to be of the same order as drag on Explorer IX and is much larger than the changes due to earth-reflected radiation, earth-emitted radiation, and satellite-emitted radiation. Besides being relatively small in magnitude, earth-reflected radiation and earth-emitted radiation produce forces upon the Explorer IX satellite which are essentially radial. Because of the thermal design of the satellite, the temperature of surface elements facing the sun is approximately the same as the temperature of surface elements on the opposite side of the satellite. (See ref. 10.) Therefore, the net force produced by satellite-emitted radiation is quite small.

The energy change in the satellite due to direct solar radiation depends upon the motion of the satellite with respect to the earth shadow and upon the force $\vec{F}_S$ exerted by solar radiation. The force acting on flat samples of Explorer IX material due to the incidence and reflection of radiation may be determined from reference 11 and $\vec{F}_S$ can be determined by integration over the satellite surface.

From reference 11, the force $d\vec{F}_S$ on a flat surface due to the incidence and reflection of solar radiation is

$$d\vec{F}_S = \frac{I \cos \beta}{c}\left[\vec{L} - \vec{r}(\beta)\right]dA \qquad (12)$$

where

I	incident power per unit area normal to direction of propagation
β	angle between incident ray and normal to surface
c	speed of light in a vacuum, taken as $2.997\ 93 \times 10^{10}$ cm/sec
$\vec{L}$	unit vector in direction of incident light
$\vec{r}(\beta)$	vectorial reflectance of surface at particular angle of incidence

Vectorial reflectance: A particle of electromagnetic radiation has associated with it momentum which is transferred to an absorbing or reflecting medium. If parallel light of energy E is incident on a surface at rate dE/dt the magnitude of the force exerted on the surface due to incidence as opposed to reflection is $\frac{1}{c}\frac{dE}{dt}$ in the direction of the incident light. The resultant force exerted on the surface by reflected light is dependent upon the amount of light departing in each direction. The vector summation of the rate of momentum exchange by the reflected light divided by the magnitude of the rate of momentum exchange by the incident light is vectorial reflectance. In other words, vectorial reflectance is the ratio of the vectorial summation of reflected power to the magnitude of the parallel incident power.

In reference 11, the vectorial reflectance of the Explorer IX material was evaluated by using simulated sunlight. The vectorial reflectance depended upon the angle at which the light was incident. The results given in reference 11, together with equation (12), can be used to obtain the total force on the spherical satellite.

Total direct solar radiation force: Let parallel light of intensity I illuminate a hemisphere shown in figure 3, dA be an incremental surface area element of the hemisphere, and the radius of the hemisphere which is parallel to the incident light define the Z-axis of a Cartesian coordinate system originating at the center of the hemisphere. The orientation of the X- and Y-axes is arbitrary. Points on the hemisphere can be described by the spherical coordinates ϕ and ψ, where ϕ is measured from the Z-axis and ψ is measured from the X-axis to the plane containing ϕ.

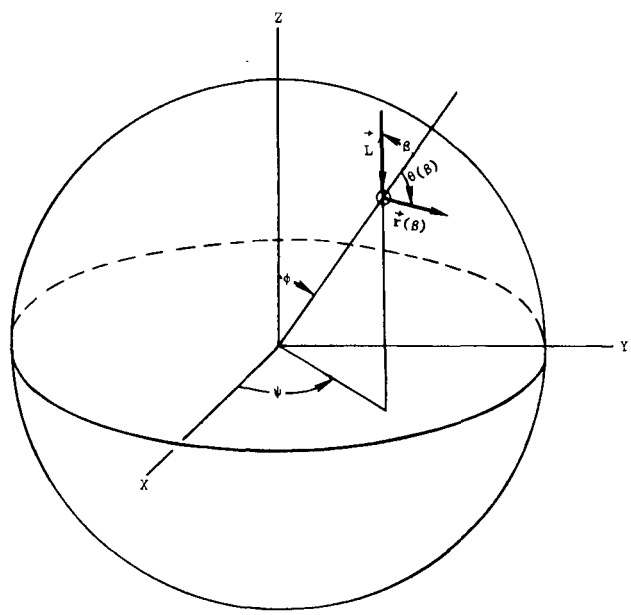

Figure 3.- Geometry of momentum transfer by solar radiation.

The force on the hemisphere can be found by resolving the force on each surface element into components normal to and parallel with the Z-axis and integrating these forces over the hemisphere. From simple geometrical considerations it can be shown that β equals ϕ, the resultant force due to symmetry is directed negatively along the Z-axis, and the z-component of $\vec{r}(\beta)$ is

$$-\left|\vec{r}(\beta)\right| \cos\left[\phi + \theta(\beta)\right] \vec{L} \tag{13}$$

Here $\theta(\beta)$, the angle between the normal to dA and $\vec{r}(\beta)$, is assumed to be in the plane of ϕ. The area element for a sphere of radius r_{sat} becomes

$$dA = r_{sat}^2 \sin \phi \, d\phi \, d\psi \tag{14}$$

Proper substitution of relation (13) and equation (14) into equation (12) and integrating over the hemisphere yields

$$\vec{F}_S = \frac{r_{sat}^2 I}{c} \left\{ \int_{\phi=0}^{\pi/2} \int_{\psi=0}^{2\pi} \cos \phi \sin \phi \, d\phi \, d\psi \right.$$

$$\left. + \int_{\phi=0}^{\pi/2} \int_{\psi=0}^{2\pi} \left|\vec{r}(\phi)\right| \cos\left[\phi + \theta(\phi)\right] \cos \phi \sin \phi \, d\phi \, d\psi \right\} \left(\vec{L}\right) \tag{15}$$

$$\vec{F}_S = \frac{\pi r_{sat}^2 I}{c} \left\{ 1 + 2 \int_{\phi=0}^{\pi/2} \left|\vec{r}(\phi)\right| \cos\left[\phi + \theta(\phi)\right] \cos \phi \sin \phi \, d\phi \right\} \left(\vec{L}\right) \tag{16}$$

The Explorer IX is uniformly covered with 2-inch-diameter dots of white paint which constitute 18 percent of its surface area. In equation (16) $\left|\vec{r}(\phi)\right| \cos\left[\phi + \theta(\phi)\right]$ can be replaced by the weighted vectorial reflectance components

$$0.82\left\{\left|\vec{r}(\phi)\right| \cos\left[\phi + \theta(\phi)\right]\right\}_{\text{aluminum}} + 0.18\left\{\left|\vec{r}(\phi)\right| \cos\left[\phi + \theta(\phi)\right]\right\}_{\text{white paint}}$$

The vectorial reflectances given in reference 11 with extrapolations to 0° and 90° incidence were substituted into the above expression. A curve of the integrand in equation (16) was then graphically integrated to yield

$$\vec{F}_S = \frac{\pi r_{sat}^2 I}{c} \left[1.028\right] \vec{L} \tag{17}$$

If the incident light is sunlight,

$$I = \frac{C_S}{r_S^2} \tag{18}$$

where

C_S solar constant at 1 astronomical unit, taken as 1.395×10^6 erg/cm^2-sec

r_S distance from earth to sun in astronomical units

Energy change per revolution: The change in energy of the satellite per revolution due to direct solar radiation force $\vec{F}_S$ may be given as follows:

$$\Delta E_S = \oint \vec{F}_S \cdot \vec{ds} \tag{19}$$

where $\vec{ds}$ is an increment of arc along the satellite orbit. Let the Z-axis of a geocentric coordinate system be the projection of the earth-sun line on the orbital plane (fig. 4). Let the angle between the earth-sun line and the Z-axis be ν and the angle between the perigee point on the orbit and the Z-axis measured in the direction of satellite motion be τ. Because of the slow variation of the direction of the sun relative to the osculating orbit during 1 revolution τ and ν are assumed constant. Due to the minute variation in the intensity of the solar flux $\left|\vec{F}_S\right|$ is assumed constant during 1 revolution when the satellite is in sunlight. If the satellite enters the earth shadow at z_{in} and exits shadow at z_{out}, it follows that

$$\Delta E_S = \left|\vec{F}_S\right| \cos \nu \left(z_{out} - z_{in}\right) \tag{20}$$

where z_{in} and z_{out} are determined from equations (35) and (36).

Although the satellite actually passes through the penumbra before going into complete shadow, for the sake of calculation, a geometrical shadow is assumed about a spherical earth. The axis of the cylindrical shadow is colinear with the earth-sun line. The intersection of the orbital plane

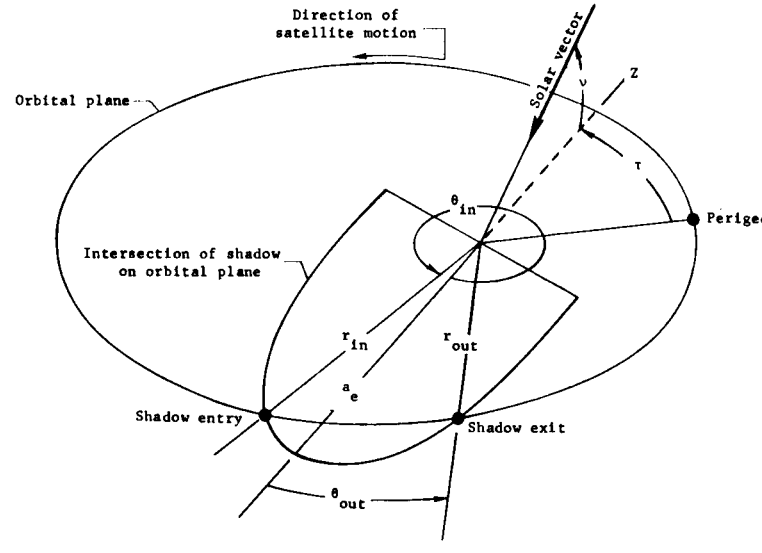

Figure 4.- Shadow and orbit ellipses.

with the cylindrical shadow of the earth is a semiellipse. The intersection of this shadow semiellipse with the orbit ellipse determines the orbital positions of shadow entry and exit.

The shadow semiellipse, centered at the center of the earth, has semiminor axis r_E and semimajor axis of $\frac{r_E}{\sin \nu}$. The radius of an ellipse with center at the origin can be written in polar coordinates as

$$r^2 = \frac{a^2b^2}{a^2\sin^2\theta + b^2\cos^2\theta} \tag{21}$$

where a and b are semimajor and semiminor axes, respectively. Then the radius of the shadow semiellipse (denoted by subscript e) may be determined from

$$r_e^2 = \frac{r_E^2}{\sin^2\theta + \sin^2\nu \cos^2\theta} \tag{22}$$

where $-90^\circ \leqq \theta \leqq 90^\circ$. The angle θ is measured from the semimajor axis of the semiellipse to r_e in the direction of satellite motion.

For the purposes of obtaining intersection points, the orbit of the satellite can be adequately expressed as an ellipse with the center of the earth at one focus as follows:

$$r = \frac{a(1 - e^2)}{1 + e \cos v} \tag{23}$$

where

$$v = \theta + \tau + 180^\circ \tag{24}$$

The angles ν and τ may be determined from considerations of the geometrical relationship between the orbital plane, the sun, and the perigee point. Shown in figure 5 is the celestial sphere upon which are shown the intersection of the orbital plane, the intersection of lines passing from the center of the earth through the sun S, the ascending node AN, the perigee P, the normal to the orbital plane $\perp$, and the projection of the earth-sun line on the orbital plane Z. The vernal equinox VE and north celestial pole NP are also illustrated.

Referring to spherical triangle S-NP-$\perp$, from the law of cosines

$$\cos(90^\circ - \nu) = \cos i \cos(90^\circ - \delta_S) + \sin i \sin(90^\circ - \delta_S)\cos(\alpha_S - \Omega + 90^\circ) \tag{25}$$

Therefore,

$$\nu = \sin^{-1}\left[\cos i \sin \delta_S - \sin i \cos \delta_S \sin(\alpha_S - \Omega)\right] \tag{26}$$

where

$$-90^{\circ} \leqq \nu \leqq 90^{\circ} \tag{27}$$

Equation (26) may be substituted into equation (22) to obtain r_e^2 as a function of θ and the known quantities.

Referring again to spherical triangle S-NP-$\perp$, from the law of cosines

$$\cos(90^{\circ} - \delta_S) = \cos(90^{\circ} - \nu)\cos i + \sin(90^{\circ} - \nu)\sin i \cos(90^{\circ} - \tau - \omega) \tag{28}$$

therefore,

$$\sin(\tau + \omega) = \frac{\sin \delta_S - \sin \nu \cos i}{\sin i \cos \nu} \tag{29}$$

In order to determine the quadrant of $\tau + \omega$, an additional relationship may be developed for $\cos(\tau + \omega)$. From spherical triangle S-$\perp$-AN,

$$\cos \lambda = \cos(90^{\circ} - \nu)\cos 90^{\circ} + \sin(90^{\circ} - \nu)\sin 90^{\circ} \cos(\tau + \omega) \tag{30}$$

therefore,

$$\cos(\tau + \omega) = \frac{\cos \lambda}{\cos \nu} \tag{31}$$

From spherical triangle S-NP-AN,

$$\cos \lambda = \cos(90^{\circ} - \delta_S)\cos 90^{\circ} + \sin(90^{\circ} - \delta_S)\sin 90^{\circ} \cos(\alpha_S - \Omega) \tag{32}$$

Simplifying equation (32) and substituting into equation (31) gives

$$\cos(\tau + \omega) = \frac{\cos \delta_S \cos(\alpha_S - \Omega)}{\cos \nu} \tag{33}$$

From equation (27), $\cos \nu$ is always positive. Since $\cos \delta_S$ is always positive, the sign of $\cos(\alpha_S - \Omega)$ is always the sign of $\cos(\tau + \omega)$. Knowing the signs of $\cos(\tau + \omega)$ and $\sin(\tau + \omega)$, the quadrant of $(\tau + \omega)$ and, therefore, the value of $(\tau + \omega)$, are uniquely determined.

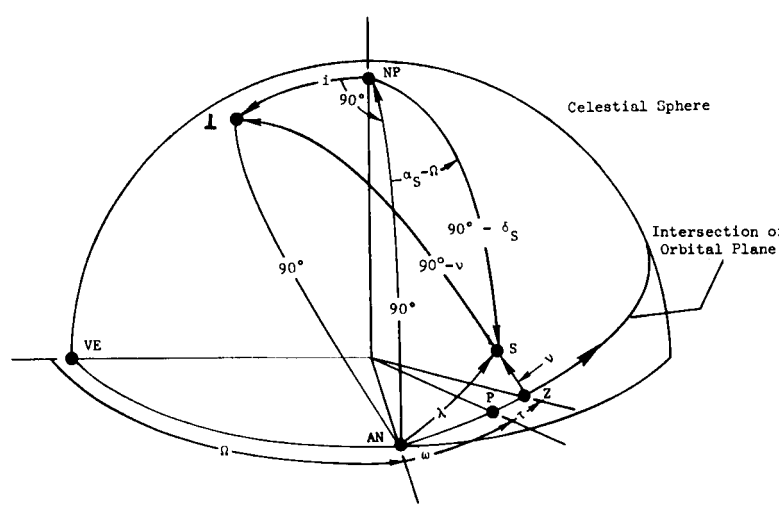

Figure 5.- Geometry for determination of τ and ν.

From equation (29),

$$\tau = \sin^{-1}\left(\frac{\sin \delta_S - \sin \nu \cos i}{\sin i \cos \nu}\right) - \omega \tag{34}$$

Equations (34), (24), and (23) may be used to obtain r as a function of θ and the known quantities.

Now r and r_e are known functions of θ. The values of θ for which $r = r_e$ were found by an iterative solution of a quartic equation. Comparisons of r and r_e were made systematically at different values of θ until the angles at which r equals r_e were found within 0.01°. If the satellite enters shadow at r_{in}, θ_{in} and exits shadow at r_{out}, θ_{out}, then

$$z_{in} = -r_{in} \cos \theta_{in} \tag{35}$$

$$z_{out} = -r_{out} \cos \theta_{out} \tag{36}$$

Energy change between epochs: Equations have now been developed for determining the energy change due to direct solar radiation during 1 revolution. In order to evaluate the energy change due to solar radiation between successive sets of orbital elements, the energy change per revolution is evaluated once daily and the total energy change is determined by numerical integration. Values of a, e, i, ω, Ω, W, α_S, and δ_S used to determine ΔE_S are assumed to vary linearly between epochs. This assumption introduces a very small error, since ω, Ω, and α_S (the most sensitive values) do, for all practical purposes, vary linearly over a time interval of the order of a week. If the satellite enters continuous sunlight, causing the energy change due to solar radiation to approach zero, or if the energy change per revolution changes sign, the energy change per revolution during that day is evaluated every 2 hours.

Calculation of Densities

If aerodynamic drag D is acting on a satellite traveling along arc s, the work W done per revolution upon the satellite by drag may be given as

$$W = \oint D \, ds \tag{37}$$

The work done is equivalent to the change of energy per revolution produced by drag ΔE_D. The drag is $\frac{1}{2}\rho \dot{s}^2 A C_D$ where ρ is the atmospheric density, $\dot{s}$ is the satellite velocity, A is the cross-sectional area, and C_D is the drag coefficient. The energy change ΔE_D is first determined in terms of true

anomaly and then put in terms of eccentric anomaly. If C_D and A are assumed constant

$$\Delta E_D = -\frac{\mu A C_D}{2} \int_{\epsilon=0}^{\epsilon=2\pi} \frac{(1 + e \cos \epsilon)^{3/2}}{(1 - e \cos \epsilon)^{1/2}} \rho \, d\epsilon \tag{38}$$

where μ is the mass of the earth times the universal gravitational constant taken as $3.986\ 135\ 271 \times 10^{20}$ dynes cm^2/gm, e is eccentricity, and ϵ is eccentric anomaly.

An equation has been derived in reference 12 for the change of semimajor axis due to drag in a spherically symmetric atmosphere from an equation similar to equation (38) with the exception that a correction factor K has been applied to yield the satellite velocity relative to an atmosphere rotating with the earth.

Assuming that

$$\rho = \rho_p \exp^{\frac{-r+r_p}{H}} \tag{39}$$

where H is a constant and the subscript p denotes values at perigee, and expanding the integrand in equation (38) as a power series in eccentricity, the expression may be replaced by Bessel functions which when in turn are replaced by their asymptotic expansions yield the following relation (see ref. 12):

$$\bar{\rho}_p = \frac{-1}{2KC_D}\left(\frac{m}{A}\right)\left(\frac{\overline{\Delta a_D}}{a}\right)\sqrt{\frac{2e}{\pi a H}}\left[1 - 2e + \frac{5e^2}{2} - \frac{H}{8ae}\left(1 - 10e + \frac{7H}{16ae}\right) + \cdots\right] \tag{40}$$

where

$$\frac{2H}{a} \leq e \leq 0.2 \tag{41}$$

and

$$K = \left(1 - \frac{r_p \omega}{\dot{s}_p} \cos i\right)^2 \tag{42}$$

Here, ω is the angular velocity of the earth and $\dot{s}_p$ can be obtained from

$$\dot{s}_p^2 = \mu\left(\frac{2}{r_p} - \frac{1}{a}\right) \tag{43}$$

The density at the perigee point of the satellite may be determined once the values of $\overline{\Delta a_D}$, m/A, H, a, e, C_D, and K are found.

The change of semimajor axis per revolution due to drag averaged between successive sets of orbital elements is $\overline{\Delta a_D}$. The average change in energy per revolution due to drag $\overline{\Delta E_D}$ is given as the difference between the total energy change and the energy change due to direct solar radiation between successive sets of orbital elements divided by the number of revolutions. The value of $\overline{\Delta a_D}$ is then determined from the following equation:

$$\overline{\Delta E_D} = \frac{\mu}{2a^2}\overline{\Delta a_D} \tag{44}$$

The greater the number of revolutions, the less is the uncertainty in $\overline{\Delta a_D}$ and, therefore, in $\bar{\rho}_p$. The only disadvantage is that due to the precession of perigee and of the ascending node, the position at which the density is measured becomes more uncertain with an increasing number of revolutions. Therefore, a time interval should be chosen such that the density is of suitable accuracy without undue sacrifice of the accuracy of time and position of the measurement.

It has been shown (ref. 13) that for a sphere in free molecular flow, the drag coefficient for diffuse reflection is

$$C_D = \frac{2\exp(-S^2)}{\sqrt{\pi}S}\left(1 + \frac{1}{2S^2}\right) + 2\left(1 + \frac{1}{S^2} - \frac{1}{4S^4}\right)\operatorname{erf}(S) + \frac{2\sqrt{\pi}}{3S_r} \tag{45}$$

The molecular speed ratio S is the ratio of the satellite speed with respect to the atmosphere to the most probable molecular speed, and S_r is the molecular speed ratio of the diffusely reflected particles. The satellite speed depends upon the orbit and the position of the satellite in that orbit. The rotation of the atmosphere must be considered in determining satellite speed with respect to the atmosphere. The atmospheric mean molecular speed at any position depends upon the temperature and molecular weight, which is determined by the heating and heat transfer in the atmosphere. The mean molecular speed of the diffusely reflected particles depends in addition upon the accommodation coefficient and temperature of the satellite. This means that C_D is, under some initial assumptions for atmospheric conditions and properties of the satellite, a function of satellite position and velocity, which are in turn functions of the orbital elements. That is, C_D should not be assumed constant and removed from the integral of equation (38).

Because of the difficulty of integrating in equation (38) with C_D a function of all its implicit variables, an investigation was made with the object of determining $\overline{C_D}$ which could be written in terms of fewer variables. Let $\overline{C_D}$ be defined by

$$\Delta E_D = -\frac{\mu A}{2}\int_{\epsilon=0}^{\epsilon=2\pi}\frac{(1+e\cos\epsilon)^{3/2}}{(1-e\cos\epsilon)^{1/2}}C_D\rho\,d\epsilon = -\frac{\mu A\overline{C_D}}{2}\int_{\epsilon=0}^{\epsilon=2\pi}\frac{(1+e\cos\epsilon)^{3/2}}{(1-e\cos\epsilon)^{1/2}}\rho\,d\epsilon \tag{46}$$

The effects of orbital parameters, thermal accommodation coefficient, satellite skin temperature, rotating atmosphere, and solar heating were investigated by choosing several sets of initial conditions and calculating $\overline{C_D}$ for a variety of orbits. It was found that the most significant variables were height of perigee and thermal accommodation coefficient. Assuming skin temperatures obtained when Explorer IX is in continuous sunlight (ref. 10) and complete thermal accommodation, the following approximate equations were determined giving $\overline{C_D}$ as a function of height of perigee h_p:

$$\overline{C_D} = 2.050 + 2.484 \times 10^{-4}\,h_p \qquad (200\text{ km} \leqq h_p \leqq 600\text{ km}) \tag{47}$$

$$\overline{C_D} = 2.134 + 1.125 \times 10^{-4}\,h_p \qquad (600\text{ km} \leqq h_p \leqq 800\text{ km}) \tag{48}$$

The value of H, which is the negative slope of a log-density—height curve, was obtained from the densities given in the 1962 U.S. Standard Atmosphere (ref. 14).

$$H = \left(-5.994 \times 10^{-5}\right)h^2 + 0.1659h + 7.1687 \qquad (200\text{ km} \leqq h \leqq 800\text{ km}) \tag{49}$$

Because H is variable, a weighted value of H was used. The quantity H is calculated at the height $h_p + \frac{3H_p}{4}$ where H_p is the value of H at h_p. (See ref. 15.) The height of perigee in kilometers is given as

$$h_p = a(1-e) - 6378.388\left(1 - \frac{\sin^2 i \sin^2\omega}{297}\right) \tag{50}$$

The position of the perigee point, which is essentially the density point, may be given in terms of the radius, right ascension, and declination of perigee as follows:

$$r_p = a(1-e) \tag{51}$$

$$\alpha_p = \Omega + \alpha \tag{52}$$

where α is the change in right ascension between the ascending node and the perigee point.

It can be shown by spherical trigonometry that

$$\alpha = \tan^{-1}(\cos i \tan \omega) \tag{53}$$

If $0 \leqq i < 90^{\circ}$, α and ω are in the same quadrant. If $90^{\circ} \leqq i < 180^{\circ}$, α is in the quadrant of $-\omega$.

Similarly, it is found that

$$\delta_p = \sin^{-1}(\sin i \sin \omega) \tag{54}$$

where

$$-90^{\circ} \leqq \delta_p \leqq 90^{\circ} \tag{55}$$

ATMOSPHERIC DENSITIES

The equations given in the section "Procedure" have been incorporated in a computing program for determination of atmospheric density from the energy decay of a satellite. Given two sets of orbital elements and the corresponding right ascension and declination of the sun, and the earth-sun distance in astronomical units, the program determines the following quantities:

(1) Total energy change due to solar radiation force between epochs

(2) Total energy change between epochs

(3) Average energy change per revolution due to drag and the corresponding change of semimajor axis per revolution due to drag

(4) Aerodynamic drag coefficient averaged over a revolution

(5) The quantity H at $h_p + \frac{3H_p}{4}$

(6) Average values of the orbital elements, the right ascension, declination, radius, and height above the geoid of the density point, and parameters associated with analysis of density

(7) Average density and $\log_{10}$ of average density

The general organization of this program is shown in figure 6.

Presented in table I are mean orbital elements computed by the Smithsonian Astrophysical Observatory using the Differential Orbit Improvement Program discussed previously. The elements are referenced to the equinox of 1950.0 and the equator of date. The elements tabulated for 1961 and 1962 are given in references 16, 17, and 18 and are based on precisely reduced Baker-Nunn photographs. At this time, precise elements are published for only 1961 and 1962.

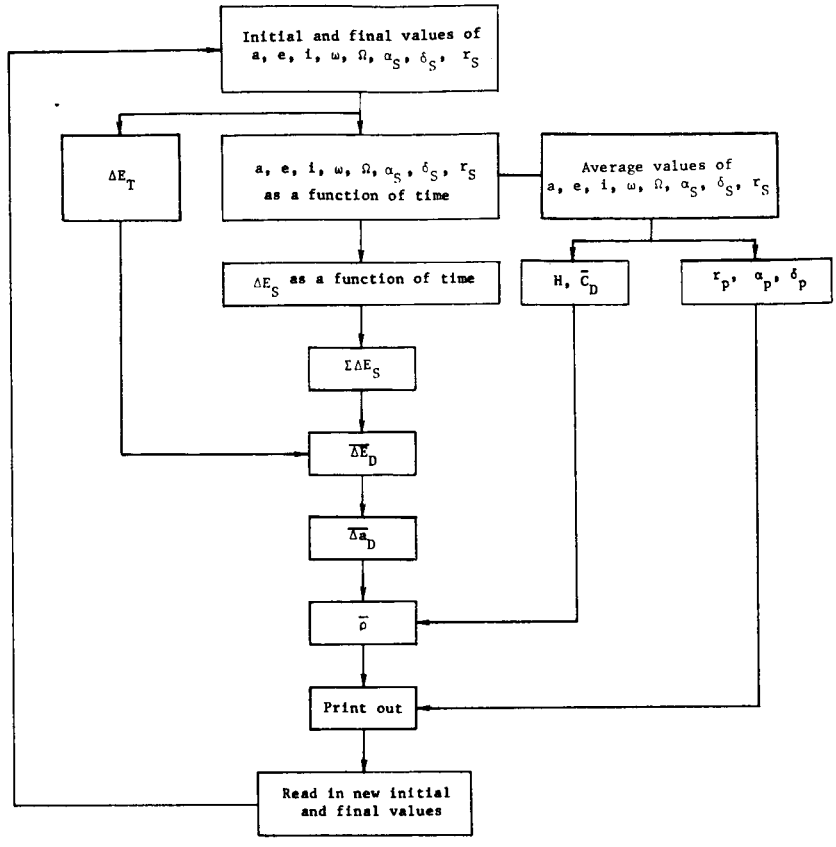

Figure 6.- Schematic diagram of computational procedure.

The elements for dates between January 1, 1963, and September 30, 1963, are given in references 19, 20, and 21 and are based upon less accurate field-reduced data. The remainder of the tabulated orbital elements are unpublished predictions which were originally used by the Smithsonian Astrophysical Observatory to predict satellite position so that subsequent observations could be made. Consequently, all these observations were obtained prior to the epoch times.

Given in table I(a) are the published orbital elements of Explorer IX. In the first column, the epoch indicates the reference time for a set of orbital elements. All times are zero Universal Time to the nearest millisecond. The second column gives the mean (anomalistic) motion in revolutions per day. The last four columns give the eccentricity, orbital inclination in degrees, argument of perigee in degrees, and right ascension of the ascending node in degrees. With the exception of the epoch, the last place in each column is generally unreliable. Table I(b) is similar to table I(a) except that the second column is semimajor axis in kilometers.

With the equations given in this paper, mean atmospheric densities and their associated time and position were computed between the successive epochs tabulated in table I. Table II gives the results of these computations. The first four columns are simply midpoints in time, radius, right ascension, and

declination of the perigee point between successive epochs. The fifth column gives $\log_{10}$ of mean atmospheric density. In the sixth column is the time interval between successive orbital elements used to infer atmospheric density.

Referring to equation (40), errors in the determination of average density may be attributed chiefly to inaccuracies in $\overline{\Delta a_D}$, $\overline{C_D}$, $H^{1/2}$, K, and the atmospheric model. Any of these factors could introduce an error on the order of 5 percent. The error in $\overline{\Delta a_D}$ is principally a function of the accuracy of orbit determination, and the accuracies of determination of energy changes by causes other than drag. The errors in orbit determination are dependent upon the number of observations, the accuracy of observations, the distribution of observations in space and time, and inadequacies in theory. The errors due to energy changes other than drag are principally dependent on errors in determination of perturbing forces acting on the satellite. Errors in $\overline{C_D}$ are principally dependent upon the inaccuracy in the estimate of the thermal accommodation coefficient. Errors in $H^{1/2}$ are dependent upon errors in the mean molecular mass and kinetic temperature. Errors in K depend principally upon errors in the rate of atmospheric rotation. Errors due to the atmospheric model could result from the choice of a radially symmetric atmosphere instead of one with a diurnal bulge.

CONCLUDING REMARKS

A specific procedure has been developed and successfully used for determination of mean atmospheric densities from changes in the orbital elements of the Explorer IX satellite. Errors in determination of mean density may be attributed chiefly to inaccuracies in the determination of energy decay due to drag, aerodynamic drag coefficient, variation of density with altitude, the rate of rotation of the atmosphere, and the assumed atmospheric model. During the development of the method, equations were obtained for the total energy of a satellite about an oblate spheroid; the solar radiation force and resultant energy changes upon Explorer IX; and the aerodynamic drag coefficient of Explorer IX as a function of height of perigee. From orbital elements derived from observations of Explorer IX, mean atmospheric densities and their associated position were deduced for the entire lifetime of the satellite.

Langley Research Center,
National Aeronautics and Space Administration,
Langley Station, Hampton, Va., March 16, 1965.

REFERENCES

1. Coffee, Claude W., Jr.; Bressette, Walter E.; and Keating, Gerald M.: Design of the NASA Lightweight Inflatable Satellites for the Determination of Atmospheric Density at Extreme Altitudes. NASA TN D-1243, 1962.

2. Staff of the Smithsonian Institution Astrophysical Observatory: Notes on the Design and Operation of Satellite Tracking Stations for Geodetic Purposes. Spec. Rept. No. 124, Smithsonian Inst. Astrophys. Obs., May 27, 1963.

3. Lassovszky, Karoly: On the Accuracy of Measurements Made Upon Films Photographed by Baker-Nunn Satellite Tracking Cameras. Smithsonian Contrib. Astrophys., vol. 6, 1963, pp. 165-173.

4. Veis, G.; and Moore, C. H.: Smithsonian Astrophysical Observatory Differential Orbit Improvement Program. Seminar Proceedings - Tracking Programs and Orbit Determination. Astronaut. Inform. (Contract No. NASw-6), Jet Propulsion Lab., C.I.T., c.1960, pp. 165-184.

5. Gaposchkin, E. M.: Differential Orbit Improvement (DØI-3). Spec. Rept. No. 161, Smithsonian Inst. Astrophys. Obs., Aug. 3, 1964.

6. Kozai, Yoshihide: The Motion of a Close Earth Satellite. Astron. J., vol. 64, no. 9, Nov. 1959, pp. 367-377.

7. Kozai, Yoshihide: On the Effects of the Sun and the Moon Upon the Motion of a Close-Earth Satellite. Smithsonian Contrib. Astrophys., vol. 6, 1963, pp. 47-49.

8. Cook, G. E.: Luni-Solar Perturbations of the Orbit of an Earth Satellite. Tech. Note No. GW 582, Brit. R.A.E., July 1961.

9. Hohl, Frank; and Wood, George P.: The Electrostatic and Electromagnetic Drag Forces on a Spherical Satellite in a Rarefied Partially Ionized Atmosphere. Rarefied Gas Dynamics, Vol. II, J. A. Laurmann, ed., Academic Press, 1963, pp. 45-64.

10. Woerner, Charles V.; and Keating, Gerald M.: Temperature Control of the Explorer IX Satellite. NASA TN D-1369, 1962.

11. Keating, Gerald M.; and Mullins, James A.: Vectorial Reflectance of the Explorer IX Satellite Material. NASA TN D-2388, 1964.

12. Cook, G. E.; King-Hele, D. G.; and Walker, Doreen M. C.: The Contraction of Satellite Orbits Under the Influence of Air Drag. I. With Spherically Symmetrical Atmosphere. Proc. Roy. Soc. (London), ser. A., vol. 257, no. 1289, Sept. 6, 1960, pp. 224-249.

13. Stalder, Jackson R.; and Zurick, Vernon J.: Theoretical Aerodynamic Characteristics of Bodies in a Free-Molecule-Flow Field. NACA TN 2423, 1951.

14. Anon.: U.S. Standard Atmosphere, 1962. NASA, U.S. Air Force, and U.S. Weather Bur., Dec. 1962.

15. Cook, G. E.; and King-Hele, D. G.: The Contraction of Satellite Orbits Under the Influence of Air Drag. IV. With Scale Height Dependent on Altitude. Proc. Roy. Soc. (London), ser. A., vol. 275, no. 1363, Oct. 29, 1963, pp. 357-390.

16. Anon.: Satellite Orbital Data No. E-2. Spec. Rept. No. 119, Smithsonian Inst. Astrophys. Obs., Mar. 15, 1963.

17. Anon.: Satellite Orbital Data No. E-3. Spec. Rept. No. 141, Smithsonian Inst. Astrophys. Obs., Jan. 30, 1964.

18. Anon.: Satellite Orbital Data No. E-4. Spec. Rept. No. 158, Smithsonian Inst. Astrophys. Obs., July 10, 1964.

19. Anon.: Satellite Orbital Data. Spec. Rept. No. 142, Smithsonian Inst. Astrophys. Obs., Jan. 31, 1964.

20. Anon.: Satellite Orbital Data. Spec. Rept. No. 159, Smithsonian Inst. Astrophys. Obs., July 17, 1964.

21. Anon.: Satellite Orbital Data. Spec. Rept. No. 160, Smithsonian Inst. Astrophys. Obs., July 27, 1964.

TABLE I.- ORBITAL ELEMENTS OF EXPLORER IX

(a) With mean motion

Epoch	n, rev/day	e	i, deg	ω, deg	Ω, deg
1961					
FEB. 18.0	12.159994	.122108	38.862	106.541	165.730
FEB. 24.0	12.160292	.121341	38.862	134.998	143.890
MARCH 2.0	12.160617	.120480	38.866	163.558	122.063
MARCH 8.0	12.161010	.119687	38.869	192.165	100.242
MARCH 14.0	12.161297	.118986	38.867	220.821	78.428
MARCH 20.0	12.161522	.118344	38.866	249.468	56.615
MARCH 26.0	12.161944	.117738	38.863	278.144	34.807
APRIL 1.0	12.162977	.117234	38.862	306.795	13.000
APRIL 7.0	12.163538	.116881	38.860	335.509	351.196
APRIL 13.0	12.163832	.116659	38.858	4.159	329.395
APRIL 19.0	12.164225	.116456	38.853	32.734	307.596
APRIL 25.0	12.164546	.116222	38.849	61.232	285.799
MAY 1.0	12.165008	.115817	38.846	89.729	263.995
MAY 7.0	12.165407	.115283	38.846	118.218	242.198
MAY 13.0	12.165598	.114733	38.849	146.780	220.407
MAY 19.0	12.165919	.114211	38.850	175.391	198.621
MAY 25.0	12.166781	.113759	38.850	204.072	176.830
MAY 31.0	12.167636	.113316	38.846	232.757	155.036
JUNE 6.0	12.168403	.112861	38.847	261.417	133.240
JUNE 12.0	12.168695	.112425	38.845	290.068	111.444
JUNE 18.0	12.168728	.112047	38.843	318.732	89.657
JUNE 24.0	12.169191	.111744	38.841	347.356	67.877
JUNE 28.0	12.169202	.111653	38.840	6.465	53.354
JULY 4.0	12.169110	.111515	38.839	35.052	31.578
JULY 10.0	12.169129	.111363	38.835	63.571	9.804
JULY 16.0	12.169581	.111003	38.834	92.077	348.027
JULY 22.0	12.170159	.110578	38.835	120.579	326.255
JULY 28.0	12.170706	.110108	38.837	149.160	304.488
AUG. 3.0	12.170960	.109654	38.838	177.801	282.721
AUG. 9.0	12.171330	.109268	38.838	206.488	260.953
AUG. 15.0	12.172233	.108896	38.837	235.216	239.179
AUG. 21.0	12.173167	.108468	38.836	263.958	217.405
AUG. 27.0	12.173391	.108115	38.834	292.686	195.631
SEPT. 2.0	12.173522	.107873	38.831	321.419	173.863
SEPT. 8.0	12.173683	.107790	38.829	350.141	152.097
SEPT. 14.0	12.174249	.107788	38.827	18.841	130.333
SEPT. 20.0	12.174912	.107846	38.826	47.453	108.567
SEPT. 26.0	12.175328	.107798	38.823	76.001	86.797
OCT. 2.0	12.175840	.107508	38.822	104.509	65.027
OCT. 8.0	12.176234	.107084	38.823	133.048	43.257
OCT. 14.0	12.176884	.106558	38.825	161.669	21.492
OCT. 20.0	12.177272	.106081	38.828	190.377	359.725
OCT. 26.0	12.177646	.105699	38.828	219.148	337.962
NOV. 1.0	12.178390	.105418	38.830	247.968	316.201
NOV. 7.0	12.178744	.105241	38.828	276.807	294.437
NOV. 13.0	12.179341	.105172	38.827	305.640	272.671
NOV. 19.0	12.179858	.105270	38.825	334.458	250.902
NOV. 25.0	12.180497	.105536	38.822	3.239	229.132
DEC. 1.0	12.181305	.105909	38.821	31.929	207.354
DEC. 7.0	12.182381	.106221	38.816	60.527	185.568
DEC. 13.0	12.183131	.106259	38.815	89.019	163.770
DEC. 19.0	12.183618	.105978	38.816	117.552	141.969
DEC. 25.0	12.183916	.105498	38.820	146.130	120.179
DEC. 31.0	12.184163	.104956	38.821	174.803	98.393

TABLE I.- ORBITAL ELEMENTS OF EXPLORER IX - Continued

(a) With mean motion - Continued

Epoch	n, rev/day	e	i, deg	ω, deg	Ω, deg
1962					
JAN. 6.0	12.184244	.104532	38.823	203.569	76.607
JAN. 12.0	12.184313	.104206	38.825	232.423	54.828
JAN. 18.0	12.184509	.104055	38.828	261.303	33.052
JAN. 24.0	12.184829	.103999	38.826	290.192	11.274
JAN. 30.0	12.185301	.104052	38.824	319.051	349.495
FEB. 5.0	12.185822	.104287	38.822	347.887	327.712
FEB. 11.0	12.186501	.104625	38.820	16.659	305.924
FEB. 17.0	12.187274	.104996	38.819	45.338	284.132
FEB. 23.0	12.188079	.105225	38.817	73.948	262.330
MARCH 1.0	12.188897	.105212	38.817	102.546	240.522
MARCH 7.0	12.189551	.104976	38.817	131.186	218.710
MARCH 13.0	12.189927	.104650	38.818	159.871	196.907
MARCH 19.0	12.190462	.104391	38.820	188.661	175.104
MARCH 25.0	12.191575	.104239	38.822	217.511	153.294
MARCH 31.0	12.192739	.104248	38.825	246.375	131.483
APRIL 6.0	12.193438	.104341	38.826	275.276	109.662
APRIL 12.0	12.194139	.104456	38.828	304.160	87.840
APRIL 18.0	12.195059	.104613	38.826	333.021	66.015
APRIL 24.0	12.196353	.104839	38.825	1.851	44.187
APRIL 30.0	12.197255	.105128	38.821	30.632	22.353
MAY 6.0	12.198000	.105478	38.820	59.347	0.512
MAY 12.0	12.198781	.105696	38.820	88.008	338.666
MAY 18.0	12.199658	.105804	38.820	116.654	316.816
MAY 24.0	12.200623	.105780	38.820	145.363	294.959
MAY 30.0	12.201604	.105727	38.822	174.122	273.099
JUNE 5.0	12.202724	.105792	38.825	202.948	251.233
JUNE 11.0	12.203886	.105921	38.828	231.789	229.358
JUNE 17.0	12.204788	.106179	38.828	260.645	207.474
JUNE 23.0	12.205369	.106431	38.829	289.490	185.581
JUNE 29.0	12.205948	.106639	38.830	318.378	163.687
JULY 5.0	12.206400	.106860	38.832	347.271	141.792
JULY 11.0	12.206992	.107148	38.829	16.131	119.898
JULY 17.0	12.207645	.107524	38.828	44.926	98.001
JULY 23.0	12.208470	.107871	38.827	73.664	76.095
JULY 29.0	12.209356	.108127	38.828	102.358	54.186
AUG. 4.0	12.210176	.108265	38.830	131.085	32.270
AUG. 10.0	12.211087	.108278	38.832	159.865	10.349
AUG. 16.0	12.212086	.108332	38.835	188.706	348.425
AUG. 22.0	12.213376	.108476	38.836	217.633	326.491
AUG. 28.0	12.214674	.108708	38.838	246.558	304.551
SEPT. 3.0	12.215543	.109061	38.841	275.502	282.599
SEPT. 9.0	12.217159	.109460	38.843	304.452	260.642
SEPT. 15.0	12.218449	.109914	38.843	333.408	238.678
SEPT. 21.0	12.219882	.110415	38.841	2.349	216.706
SEPT. 27.0	12.221432	.111025	38.838	31.232	194.722
OCT. 3.0	12.223340	.111613	38.837	60.040	172.724
OCT. 9.0	12.225180	.112123	38.838	88.773	150.715
OCT. 15.0	12.227089	.112460	38.842	117.482	128.692
OCT. 21.0	12.228650	.112604	38.848	146.274	106.657
OCT. 27.0	12.230413	.112607	38.853	175.188	84.616
NOV. 2.0	12.232321	.112628	38.857	204.191	62.576
NOV. 8.0	12.234208	.112764	38.857	233.265	40.522
NOV. 14.0	12.236100	.113090	38.858	262.355	18.456
NOV. 20.0	12.238181	.113510	38.857	291.446	356.380
NOV. 26.0	12.240252	.114060	38.860	320.526	334.287
DEC. 2.0	12.242195	.114766	38.857	349.591	312.815
DEC. 8.0	12.244377	.115494	38.853	18.590	290.065
DEC. 14.0	12.246682	.116243	38.851	47.504	267.926
DEC. 20.0	12.248947	.116891	38.852	76.350	245.770
DEC. 26.0	12.250787	.117359	38.855	105.147	223.601

TABLE I.- ORBITAL ELEMENTS OF EXPLORER IX - Continued

(a) With mean motion - Concluded

Epoch	n, rev/day	e	i, deg	ω, deg	Ω, deg
1963					
JAN. 1.0	12.251600	.117510	38.855	133.940	201.421
JAN. 7.0	12.252500	.117640	38.866	163.040	179.246
JAN. 13.0	12.253680	.117610	38.871	192.110	157.042
JAN. 19.0	12.255510	.117670	38.873	221.292	134.854
JAN. 25.0	12.257260	.117970	38.876	250.540	112.654
JAN. 31.0	12.259100	.118200	38.875	279.800	90.440
FEB. 6.0	12.261390	.118950	38.882	308.990	68.215
FEB. 12.0	12.263770	.119630	38.883	338.183	45.986
FEB. 18.0	12.266260	.120210	38.879	7.350	23.730
FEB. 24.0	12.268670	.121110	38.872	36.480	1.456
MARCH 2.0	12.271100	.121740	38.873	65.541	339.167
MARCH 8.0	12.273570	.122310	38.875	94.570	316.854
MARCH 14.0	12.276510	.122610	38.875	123.581	294.544
MARCH 20.0	12.279260	.122830	38.886	152.678	272.190
MARCH 26.0	12.282110	.122950	38.885	181.876	249.839
APRIL 1.0	12.285010	.123180	38.889	211.163	227.476
APRIL 7.0	12.288160	.123480	38.893	240.502	205.087
APRIL 13.0	12.291240	.123970	38.894	269.834	182.691
APRIL 19.0	12.294604	.124380	38.900	299.147	160.268
APRIL 25.0	12.297430	.124940	38.901	328.453	137.837
MAY 1.0	12.299960	.125600	38.905	357.790	115.382
MAY 7.0	12.304060	.126110	38.903	27.110	92.915
MAY 13.0	12.306320	.126640	38.903	56.424	70.432
MAY 19.0	12.314130	.127020	38.902	85.717	47.911
MAY 25.0	12.317960	.127400	38.900	115.020	25.379
MAY 31.0	12.322190	.127660	38.901	144.341	2.811
JUNE 6.0	12.326830	.127810	38.912	173.760	340.214
JUNE 12.0	12.332360	.127850	38.909	203.268	317.605
JUNE 18.0	12.337450	.128170	38.912	232.818	294.966
JUNE 24.0	12.341440	.128410	38.915	262.365	272.309
JUNE 30.0	12.344920	.128980	38.918	291.990	249.623
JULY 6.0	12.347987	.129370	38.922	321.510	226.915
JULY 12.0	12.351792	.129780	38.923	351.115	204.195
JULY 18.0	12.355935	.130320	38.925	20.752	181.467
JULY 24.0	12.361839	.130830	38.925	50.360	158.714
JULY 30.0	12.367870	.131210	38.919	79.983	135.915
AUG. 5.0	12.375603	.131550	38.924	109.580	113.103
AUG. 11.0	12.382150	.131200	38.925	139.160	90.240
AUG. 17.0	12.387800	.131500	38.919	168.830	67.370
AUG. 23.0	12.398140	.131490	38.930	198.794	44.436
AUG. 29.0	12.404170	.131530	38.928	228.760	21.450
SEPT. 4.0	12.417790	.131700	38.938	258.750	358.460
SEPT. 10.0	12.425580	.131700	38.945	288.700	335.430
SEPT. 16.0	12.436760	.132150	38.942	318.850	312.320
SEPT. 22.0	12.454900	.132200	38.923	349.200	289.210
SEPT. 26.0	12.473530	.131600	38.930	9.100	273.700

TABLE I.- ORBITAL ELEMENTS OF EXPLORER IX - Concluded

(b) With semimajor axis

Epoch	a, km	e	i, deg	ω, deg	Ω, deg
1963					
SEPT. 26.0	7852.5669	.131600	38.930	9.100	273.700
OCT. 1.0	7845.4729	.131490	38.951	34.158	254.291
OCT. 8.0	7839.6069	.132010	38.956	69.209	227.111
OCT. 15.0	7828.7819	.133560	38.938	104.667	199.698
OCT. 19.0	7818.8660	.130886	38.939	125.258	183.917
OCT. 26.0	7804.1389	.129706	38.939	161.112	156.319
NOV. 2.0	7789.9409	.128173	38.957	197.033	128.528
NOV. 9.0	7773.7079	.126771	38.992	233.383	100.585
NOV. 16.0	7756.7869	.125452	38.964	270.099	72.443
NOV. 24.0	7738.1760	.124398	38.960	312.325	40.046
DEC. 1.0	7720.4029	.124019	38.960	349.687	11.462
DEC. 7.0	7703.2549	.122791	38.958	21.544	346.795
DEC. 12.0	7689.8359	.122757	39.003	48.588	326.098
DEC. 17.0	7676.5609	.120772	38.948	75.161	305.296
DEC. 23.0	7661.6589	.119657	38.947	107.474	280.175
DEC. 30.0	7645.4559	.117921	38.953	145.502	250.684
1964					
JAN. 3.0	7634.3359	.116690	38.954	167.455	233.744
JAN. 11.0	7610.6199	.114210	38.964	211.668	199.597
JAN. 17.0	7591.1629	.112310	38.963	245.339	173.761
JAN. 25.0	7565.9399	.110030	38.967	290.692	139.007
FEB. 4.0	7532.8420	.107810	38.963	347.947	94.982
FEB. 10.0	7505.0839	.104990	38.951	22.422	68.279
FEB. 23.0	7433.5900	.098400	38.947	98.948	9.066
MARCH 1.0	7376.7449	.091926	38.950	141.046	336.387
MARCH 8.0	7312.5769	.083690	38.949	184.404	302.730
MARCH 14.0	7256.7180	.077040	38.959	222.812	273.125
MARCH 22.0	7182.5720	.068716	38.925	276.095	232.484
MARCH 29.0	7090.5769	.057570	38.940	324.202	195.609

TABLE II.- MEAN DENSITIES AND THEIR ASSOCIATED TIME AND POSITION OF MEASUREMENT AND TIME INTERVAL OVER WHICH DENSITIES ARE AVERAGED

Epoch	α_p, deg	δ_p, deg	r_p, km	$\log_{10}(\rho, g/cm^3)$	Time interval, days
1961					
FEB. 21.0	282.213	32.625	7014.742	-16.39	6.0
MARCH -1.0	288.146	18.698	7021.124	-16.41	6.0
MARCH 5.0	289.488	1.344	7027.591	-16.43	6.0
MARCH 11.0	290.545	-16.254	7033.426	-16.51	6.0
MARCH 17.0	295.709	-30.991	7038.690	-16.52	6.0
MARCH 23.0	307.775	-38.595	7043.549	-16.42	6.0
APRIL -2.0	321.878	-35.439	7047.700	-16.25	6.0
APRIL 4.0	330.005	-23.179	7050.814	-16.38	6.0
APRIL 10.0	332.342	-6.361	7052.945	-16.51	6.0
APRIL 16.0	333.056	11.449	7054.509	-16.49	6.0
APRIL 22.0	336.548	27.300	7056.115	-16.52	6.0
MAY -2.0	346.503	37.388	7058.515	-16.46	6.0
MAY 4.0	0.808	37.494	7062.097	-16.50	6.0
MAY 10.0	10.933	27.547	7066.311	-16.66	6.0
MAY 16.0	14.567	11.734	7070.492	-16.69	6.0
MAY 22.0	15.328	-6.085	7074.151	-16.56	6.0
MAY 28.0	17.627	-22.937	7077.391	-16.61	6.0
JUNE 3.0	25.642	-35.291	7080.661	-16.66	6.0
JUNE 9.0	39.692	-38.615	7084.012	-16.69	6.0
JUNE 15.0	51.864	-31.168	7087.198	-16.65	6.0
JUNE 21.0	57.153	-16.520	7089.820	-16.46	6.0
JUNE 26.0	58.204	-1.941	7091.301	-16.69	4.0
JULY 1.0	58.914	12.843	7092.231	-16.82	6.0
JULY 7.0	62.867	28.392	7093.402	-16.77	6.0
JULY 13.0	73.427	37.804	7095.354	-16.55	6.0
JULY 19.0	87.745	36.998	7098.287	-16.51	6.0
JULY 25.0	97.322	26.388	7101.641	-16.57	6.0
AUG. -0.	100.591	10.273	7105.173	-16.83	6.0
AUG. 6.0	101.347	-7.579	7108.404	-16.84	6.0
AUG. 12.0	104.024	-24.215	7111.182	-16.60	6.0
AUG. 18.0	112.748	-35.994	7114.017	-16.56	6.0
AUG. 24.0	127.146	-38.352	7116.908	-16.75	6.0
SEPT. -1.0	138.845	-30.031	7119.213	-16.72	6.0
SEPT. 5.0	143.663	-14.909	7120.453	-16.75	6.0
SEPT. 11.0	144.716	2.814	7120.650	-16.60	6.0
SEPT. 17.0	146.415	20.048	7120.187	-16.60	6.0
SEPT. 23.0	153.062	33.514	7119.936	-16.75	6.0
OCT. -1.0	166.239	38.822	7121.104	-16.65	6.0
OCT. 5.0	179.326	33.332	7123.776	-16.66	6.0
OCT. 11.0	185.854	19.766	7127.363	-16.54	6.0
OCT. 17.0	187.509	2.494	7131.163	-16.71	6.0
OCT. 23.0	188.604	-15.223	7134.441	-16.78	6.0
NOV. -2.0	193.609	-30.289	7136.868	-16.59	6.0
NOV. 4.0	205.577	-38.423	7138.481	-16.83	6.0
NOV. 10.0	220.043	-35.766	7139.276	-16.68	6.0
NOV. 16.0	228.653	-23.743	7138.943	-16.79	6.0
NOV. 22.0	231.281	-6.968	7137.265	-16.80	6.0
DEC. -2.0	232.112	10.917	7134.433	-16.75	6.0
DEC. 4.0	235.582	26.914	7131.332	-16.54	6.0
DEC. 10.0	245.412	37.215	7129.580	-16.68	6.0
DEC. 16.0	259.728	37.593	7130.307	-16.87	6.0
DEC. 22.0	270.045	27.841	7133.190	-16.85	6.0
DEC. 28.0	273.835	12.101	7137.160	-16.76	6.0

TABLE II.- MEAN DENSITIES AND THEIR ASSOCIATED TIME AND POSITION OF MEASUREMENT AND TIME INTERVAL OVER WHICH DENSITIES ARE AVERAGED - Continued

Epoch	α_p, deg	δ_p, deg	r_p, km	$\log_{10}(\rho, g/cm^3)$	Time interval, days
1962					
JAN. 3.0	274.682	-5.742	7140.948	-16.99	6.0
JAN. 9.0	277.043	-22.700	7143.911	-17.18	6.0
JAN. 15.0	285.195	-35.206	7145.761	-17.09	6.0
JAN. 21.0	299.524	-38.596	7146.486	-16.97	6.0
JAN. 27.0	311.932	-31.062	7146.343	-16.85	6.0
FEB. 2.0	317.344	-16.265	7145.000	-16.88	6.0
FEB. 8.0	318.589	1.425	7142.480	-16.83	6.0
FEB. 14.0	320.114	18.835	7139.369	-16.80	6.0
FEB. 20.0	326.299	32.745	7136.668	-16.71	6.0
MARCH -2.0	339.176	38.795	7135.490	-16.65	6.0
MARCH 4.0	352.646	34.000	7136.196	-16.71	6.0
MARCH 10.0	359.665	20.782	7138.235	-16.90	6.0
MARCH 16.0	1.527	3.593	7140.390	-16.86	6.0
MARCH 22.0	2.565	-14.228	7141.707	-16.59	6.0
MARCH 28.0	7.243	-29.578	7141.832	-16.60	6.0
APRIL 3.0	18.853	-38.237	7141.062	-16.83	6.0
APRIL 9.0	33.449	-36.173	7139.960	-16.74	6.0
APRIL 15.0	42.431	-24.503	7138.559	-16.60	6.0
APRIL 21.0	45.247	-7.842	7136.600	-16.46	6.0
APRIL 27.0	46.057	10.098	7134.119	-16.67	6.0
MAY 3.0	49.345	26.307	7131.251	-16.84	6.0
MAY 9.0	58.983	36.985	7128.690	-16.86	6.0
MAY 15.0	73.407	37.765	7127.068	-16.80	6.0
MAY 21.0	84.021	28.233	7126.374	-16.75	6.0
MAY 27.0	87.981	12.538	7126.302	-16.79	6.0
JUNE 2.0	88.829	-5.337	7125.845	-16.77	6.0
JUNE 8.0	91.040	-22.365	7124.628	-16.78	6.0
JUNE 14.0	98.913	-35.010	7122.685	-16.78	6.0
JUNE 20.0	113.014	-38.649	7120.360	-16.78	6.0
JUNE 26.0	125.445	-31.349	7118.302	-16.81	6.0
JULY 2.0	130.936	-16.644	7116.397	-16.91	6.0
JULY 8.0	132.170	1.066	7114.166	-16.85	6.0
JULY 14.0	133.624	18.571	7111.279	-16.92	6.0
JULY 20.0	139.729	32.621	7108.112	-16.89	6.0
JULY 26.0	152.587	38.800	7105.378	-16.90	6.0
AUG. 1.0	166.099	34.059	7103.478	-16.99	6.0
AUG. 7.0	173.123	20.818	7102.541	-16.91	6.0
AUG. 13.0	174.924	3.582	7101.904	-16.88	6.0
AUG. 19.0	175.889	-14.282	7100.672	-16.72	6.0
AUG. 25.0	180.527	-29.656	7098.673	-16.75	6.0
SEPT. -0.	192.112	-38.277	7095.847	-16.73	6.0
SEPT. 6.0	206.633	-36.118	7092.372	-16.65	6.0
SEPT. 12.0	215.488	-24.337	7088.491	-16.58	6.0
SEPT. 18.0	218.190	-7.571	7084.163	-16.56	6.0
SEPT. 24.0	218.940	10.437	7079.163	-16.57	6.0
OCT. -0.	222.257	26.636	7073.727	-16.48	6.0
OCT. 6.0	232.007	37.159	7068.635	-16.52	6.0
OCT. 12.0	246.371	37.645	7064.542	-16.45	6.0
OCT. 18.0	256.693	27.841	7061.959	-16.42	6.0
OCT. 24.0	260.407	11.949	7060.735	-16.35	6.0
NOV. -1.0	261.171	-6.059	7059.933	-16.39	6.0
NOV. 5.0	263.534	-23.108	7058.578	-16.44	6.0
NOV. 11.0	271.843	-35.514	7056.014	-16.49	6.0
NOV. 17.0	286.251	-38.524	7052.283	-16.44	6.0
NOV. 23.0	298.328	-30.511	7047.629	-16.45	6.0
DEC. -1.0	303.638	-15.345	7041.864	-16.51	6.0
DEC. 5.0	304.628	2.565	7035.372	-16.44	6.0
DEC. 11.0	305.865	20.004	7028.641	-16.42	6.0
DEC. 17.0	312.443	33.607	7022.214	-16.43	6.0
DEC. 23.0	325.646	38.850	7016.994	-16.53	6.0

TABLE II.- MEAN DENSITIES AND THEIR ASSOCIATED TIME AND POSITION OF MEASUREMENT AND TIME INTERVAL OVER WHICH DENSITIES ARE AVERAGED - Continued

Epoch	α_p, deg	δ_p, deg	r_p, km	$\log_{10}(\rho, g/cm^3)$	Time interval, days
1963					
JAN. -2.0	338.558	33.079	7014.028	-16.68	6.0
JAN. 4.0	344.816	19.144	7012.585	-16.57	6.0
JAN. 10.0	346.256	1.523	7011.791	-16.48	6.0
JAN. 16.0	347.333	-16.377	7011.098	-16.41	6.0
JAN. 22.0	352.759	-31.317	7008.985	-16.54	6.0
JAN. 28.0	5.345	-38.711	7006.195	-16.56	6.0
FEB. 3.0	19.544	-34.866	7001.516	-16.40	6.0
FEB. 9.0	27.231	-21.880	6994.948	-16.36	6.0
FEB. 15.0	29.210	-4.537	6989.019	-16.33	6.0
FEB. 21.0	29.984	13.547	6982.211	-16.37	6.0
MARCH -1.0	34.190	29.196	6975.219	-16.38	6.0
MARCH 5.0	45.313	38.183	6969.527	-16.37	6.0
MARCH 11.0	59.642	36.382	6965.051	-16.23	6.0
MARCH 17.0	68.456	24.770	6961.911	-16.24	6.0
MARCH 23.0	71.041	7.949	6959.504	-16.21	6.0
APRIL -2.0	71.652	-10.281	6957.029	-16.22	6.0
APRIL 4.0	74.981	-26.765	6953.785	-16.19	6.0
APRIL 10.0	85.092	-37.369	6949.477	-16.22	6.0
APRIL 16.0	99.842	-37.442	6944.694	-16.15	6.0
APRIL 22.0	109.986	-26.955	6939.684	-16.21	6.0
MAY -2.0	113.319	-10.509	6933.840	-16.15	6.0
MAY 4.0	113.897	7.781	6927.958	-15.93	6.0
MAY 10.0	116.473	24.728	6922.080	-15.85	6.0
MAY 16.0	125.389	36.444	6916.588	-15.92	6.0
MAY 22.0	139.875	38.150	6911.961	-16.06	6.0
MAY 28.0	150.926	28.902	6907.919	-16.01	6.0
JUNE 3.0	154.917	12.978	6904.639	-15.95	6.0
JUNE 9.0	155.548	-5.334	6901.984	-15.85	6.0
JUNE 15.0	157.616	-22.770	6898.579	-15.90	6.0
JUNE 21.0	165.710	-35.500	6894.675	-16.04	6.0
JUNE 27.0	180.152	-38.555	6890.081	-16.11	6.0
JULY 3.0	192.087	-30.226	6885.068	-16.15	6.0
JULY 9.0	196.704	-14.623	6880.628	-15.93	6.0
JULY 15.0	197.454	3.724	6875.398	-15.86	6.0
JULY 21.0	199.168	21.429	6869.386	-15.75	6.0
JULY 27.0	206.575	34.763	6863.660	-15.78	6.0
AUG. 2.0	220.645	38.761	6858.271	-15.66	6.0
AUG. 8.0	232.991	31.239	6855.672	-15.75	6.0
AUG. 14.0	238.022	15.991	6853.618	-15.83	6.0
AUG. 20.0	238.871	-2.392	6849.526	-15.51	6.0
AUG. 26.0	240.433	-20.445	6845.473	-15.48	6.0
SEPT. 1.0	247.587	-34.306	6841.032	-15.61	6.0
SEPT. 7.0	261.722	-38.844	6837.350	-15.66	6.0
SEPT. 13.0	274.561	-31.500	6832.100	-15.47	6.0
SEPT. 19.0	280.004	-15.979	6824.767	-15.24	6.0
SEPT. 24.0	280.789	-0.538	6820.212	-15.04	4.0

TABLE II.- MEAN DENSITIES AND THEIR ASSOCIATED TIME AND POSITION OF MEASUREMENT AND TIME INTERVAL OVER WHICH DENSITIES ARE AVERAGED - Concluded

Epoch	α_p, deg	δ_p, deg	r_p, km	$\log_{10}(\rho, g/cm^3)$	Time interval, days
1963					
OCT. -1.5	281.136	13.395	6816.521	-15.18	5.0
OCT. 4.5	285.242	29.555	6809.285	-15.43	7.0
OCT. 11.5	299.469	38.881	6793.931	-15.14	7.0
OCT. 17.0	312.707	34.735	6789.334	-14.92	4.0
OCT. 22.5	319.910	22.125	6793.695	-15.00	7.0
NOV. -1.5	321.703	0.585	6791.693	-15.01	7.0
NOV. 5.5	323.305	-21.260	6789.860	-14.95	7.0
NOV. 12.5	333.517	-36.679	6785.960	-14.94	7.0
NOV. 20.0	352.769	-35.889	6779.627	-14.96	8.0
DEC. -2.5	2.437	-17.748	6769.246	-14.91	7.0
DEC. 4.0	3.495	3.527	6760.151	-14.85	6.0
DEC. 9.5	5.060	21.186	6751.610	-14.88	5.0
DEC. 14.5	11.180	33.691	6747.658	-14.88	5.0
DEC. 20.0	24.423	38.935	6747.172	-14.91	6.0
DEC. 26.5	38.986	30.360	6744.399	-14.94	7.0
1964					
JAN. 1.0	43.508	14.533	6743.694	-14.86	4.0
JAN. 7.0	44.127	-5.993	6742.463	-14.83	8.0
JAN. 14.0	47.987	-28.097	6740.014	-14.80	6.0
JAN. 21.0	63.825	-38.937	6736.044	-14.81	8.0
FEB. -1.0	83.233	-24.202	6727.111	-14.79	10.0
FEB. 7.0	85.666	3.257	6718.945	-14.64	6.0
FEB. 16.5	92.843	33.238	6709.743	-14.57	13.0
MARCH -2.5	119.306	32.986	6700.469	-14.40	7.0
MARCH 4.5	125.957	10.761	6699.741	-14.35	7.0
MARCH 11.0	126.694	-14.581	6699.217	-14.36	6.0
MARCH 18.0	137.069	-36.053	6693.492	-14.38	8.0
MARCH 25.5	160.787	-32.917	6685.950	-14.25	7.0

NASA-Langley, 1965 L-4343